

IMPACT OF ORBITAL ECCENTRICITY ON THE DETECTION OF TRANSITING EXTRASOLAR PLANETS

CHRISTOPHER J. BURKE

Space Telescope Science Institute, 3700 San Martin Dr., Baltimore, MD, 21218

(Received 2007 November 09)

Submitted for publication in the Astrophysical Journal

ABSTRACT

For extrasolar planets with orbital periods, $P > 10$ days, radial velocity surveys find non-circular orbital eccentricities are common, $\langle e \rangle \sim 0.3$. Future surveys for extrasolar planets using the transit technique will also have sensitivity to detect these longer period planets. Orbital eccentricity affects the detection of extrasolar planets using the transit technique in two opposing ways: an enhancement in the probability for the planet to transit near pericenter and a reduction in the detectability of the transit due to a shorter transit duration. For an eccentricity distribution matching the currently known extrasolar planets with $P > 10$ day, the probability for the planet to transit is ~ 1.25 times higher than the equivalent circular orbit and the average transit duration is ~ 0.88 times shorter than the equivalent circular orbit. These two opposing effects nearly cancel for an idealized field transit survey with independent photometric measurements that are dominated by Poisson noise. The net effect is a modest $\sim 4\%$ increase in the transiting planet yield compared to assuming all planets have circular orbits. When intrinsic variability of the star or correlated photometric measurements are the dominant source of noise, the transit detectability is independent of the transit duration. In this case the transit yield is $\sim 25\%$ higher than that predicted under the assumption of circular orbits. Since the Kepler search for Earth-sized planets in the habitable zone of a Solar-type star is limited by intrinsic variability, the Kepler mission is expected to have a $\sim 25\%$ higher planet yield than that predicted for circular orbits if the Earth-sized planets have an orbital eccentricity distribution similar to the currently known Jupiter-mass planets.

Subject headings: eclipses — planetary systems — techniques: photometric

1. INTRODUCTION

The known extrasolar planets possess a broad distribution of orbital eccentricity (Butler et al. 2006) (see Figure 1). The short period, Hot Jupiter ($P < 10$ day) planets predominately have circular orbits. However, at longer orbital periods circular orbits become a minority and the median eccentricity for extrasolar planets $e \sim 0.3$. At the extreme eccentricity end, there are three planets, HD 80606b (Naef et al. 2001), HD 20782b (Jones et al. 2006), and HD 4113b (Tamuz et al. 2007), having $e > 0.9$. HD 80606b comes closer to its stellar host ($a = 0.033$ AU) than many of the circular orbit Hot Jupiter planets. Ford & Rasio (2007) recently reviewed the various mechanisms invoked to explain the distribution of eccentricities for the known extrasolar planets. Interactions with a stellar companion, planetary companion, passing star, gaseous disk, planetesimal disk, and stellar jets have all been proposed to modify the orbital eccentricity of extrasolar planets.

Limited discussions in the literature have been given to the impact orbital eccentricity has on a transit survey for extrasolar planets. Tingley & Sackett (2005) discuss the impact of eccentricity on their η parameter (η is the ratio of the observed transit duration to an estimate of the transit duration). As expected, they find transits occur near pericenter (apocenter) are shorter (longer) in duration than the circular orbit case, and they show that the transit duration of an eccentric is typically shorter than a circular orbit of the same period. However, their discussion was focused on the impact of orbital eccentricity on their η parameter. Moutou et al. (2006) also discuss

how the transit duration is affected by orbital eccentricity, but they do not quantify the impact this will have on transit surveys. Recently, Barnes (2007) derives the probability for a planet on an eccentric orbit to transit and conclude that the photometric precision of current surveys and future surveys, such as Kepler, is insufficient to determine the orbital eccentricity solely from the light curve. Barnes (2007) concludes that without knowledge of the eccentricity from radial velocity data or independent measurement of the stellar host radius, the habitability of planets detected with Kepler will remain unknown.

Neglecting the impact eccentricity has on transit detections is justified for the current sample of transiting planets given the predominance of circular orbits for the Hot Jupiters and the strong bias of transit surveys against finding long period planets on circular orbits (Gaudi et al. 2005). The announced transit for the planet orbiting HD 17156¹ with a 21 day period and eccentric orbit (Barbieri et al. 2007) is a precursor for the kinds of planets detectable in transit surveys. As transit surveys continue, longer period transiting planets may be discovered. More importantly, the recently launched COROT mission will surpass current surveys for sensitivity to longer period planets ($P \sim$ several months; Bordé et al. 2003). Also, the Kepler mission, scheduled for launch in 2009, has a goal to find Earth-sized objects at 1 AU from their host star (Borucki et al. 2004). The main purpose of this paper is to show that given the distribution of eccentricities for the currently known ex-

¹ First detected by the radial velocity technique (Fischer et al. 2007)

trasolar planets, eccentricity should not be ignored in assessing the detectability of transiting giant planets when the transit survey is sensitive to planets with $P > 10$ day.

In addition to longer period planets, the COROT and Kepler missions also will detect transiting planets with small, Earth-sized radii. The eccentricity distribution for planets less massive than the currently known Jupiter-mass planets is beginning to be explored. Ribas & Miralda-Escudé (2007) and Ford & Rasio (2007) provide tentative evidence for the tendency of lower mass planets to have lower eccentricities in the current sample of radial velocity planets. There is theoretical agreement that a proto-planetary gas disk strongly damps the eccentricity of non-gap opening embedded low-mass planets (Goldreich & Tremaine 1980; Cresswell et al. 2007). However, the theoretical models show that once the gas disk dissipates, dynamical interactions amongst the planets results in a random-walk diffusion that leads to an increasing eccentricity that takes on a Rayleigh-distribution similar to what is observed (dotted line in Figure 1; Juric & Tremaine 2007; Zhou et al. 2007). Opposing the increases in eccentricity from planet-planet scattering, late stage interactions with planetesimals can preferentially damp the eccentricities of lower mass planets enabling theoretical models to achieve the low eccentricities of the terrestrial planets of the Solar System (Raymond et al. 2006) and possibly explain the current trend of lower eccentricities for lower mass planets (Ford & Rasio 2007). Given the number of potential physical processes that can affect orbital eccentricity, it is premature to assume that the typical Earth-like planet has an eccentricity near zero like the Solar System.

In this study, § 2 reviews the observed eccentricity distribution of the known radial velocity extrasolar planets. The broad distribution of orbital eccentricity has two main effects on the sensitivity of a transit survey. First, the planet-host separation varies along an eccentric orbit, enhancing the probability to transit when the planet is relatively closer to the stellar host. § 3 quantifies the net affect on the transit probability for a population of planets with non-circular orbits. Second, the planet velocity varies along and eccentric orbit, resulting in a reduction or lengthening of the transit duration. § 4 quantifies the distribution of transit durations resulting from a population of planets on eccentric orbits. § 5 describes how the transit duration affects transit detection for transit surveys in the limit of various noise sources. § 6 concludes by quantifying the net result of the two aforementioned effects, the enhanced probability to transit and the reduced detectability, on the yield from transit surveys.

2. ECCENTRICITY DISTRIBUTION

The solid histograms in Figure 1 show the normalized distribution of eccentricities for the known extrasolar planets with $P > 10$ day (Butler et al. 2006). The top panel shows the eccentricity distribution from planets reported before November 2006 and the bottom panel shows the eccentricity distribution including more recent discoveries (September 2007). The more recent radial velocity discoveries over the last year have increased the sample of low eccentricity systems. Results from this study are given for both epochs of the observed eccentricity distribution in order to characterize how the un-

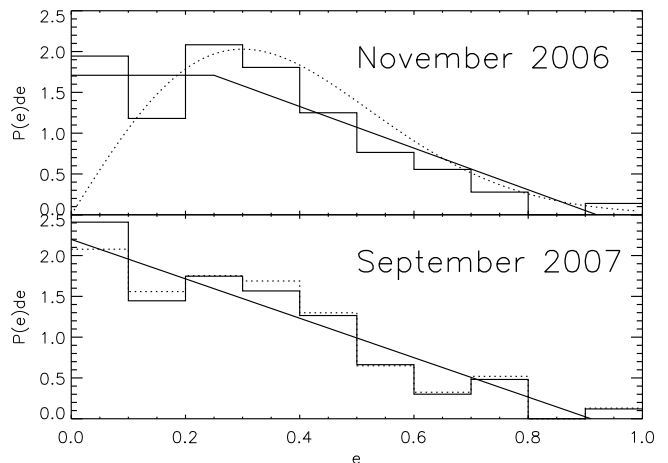


FIG. 1.— Normalized histogram of the eccentricity distribution for known extrasolar planets with $P > 10$ day. The eccentricity distribution is given for the known extrasolar planets at two epochs: November 2006 (*Top Panel*) and September 2007 (*Bottom Panel*). For this study a two-piece model parameterizes the eccentricity distribution (*solid line*). The model has 2 parameters: e_{crit} and e_{max} . The model distribution is uniform at low eccentricity up to e_{crit} ; and toward higher eccentricity, the model linearly decreases to zero-value at e_{max} . Also shown in the top panel is the Rayleigh distribution that describes the eccentricity distribution from the planet-planet scattering calculations of (Juric & Tremaine 2007) (*dotted line*). The dotted histogram in the bottom panel shows the eccentricity distribution from the latest epoch (September 2007) that excludes planets with $P < 20$ day.

certainty in the underlying orbital eccentricity distribution affects the results. No attempt was made to select planets with well determined eccentricities, avoidance of multiple planet or multiple star systems, correction for observational biases against high eccentricity planets (Cumming 2004), or evolution of orbital elements due to tidal circularization. Planets with $P < 10$ day are not included in order to examine the potential issues that future transit surveys sensitive to longer period planets will encounter. In this period regime ($P > 10$ day) high eccentricity planets are quite common ($\langle e \rangle = 0.3$ and $\sigma_e = 0.2$).

A two-piece model parameterizes the eccentricity distribution from the earlier epoch (top panel of Figure 1). The first piece at low eccentricity is flat up to e_{crit} . The second piece matches the first piece at e_{crit} , linearly decreases toward higher eccentricities, and is zero at e_{max} . The normalized two-piece model is given by the equation,

$$P(e)de = \begin{cases} \frac{2}{e_{crit} + e_{max}} & 0 \leq e \leq e_{crit} \\ \frac{2}{e_{crit} + e_{max}} \frac{(e - e_{max})}{(e_{crit} - e_{max})} & e_{crit} < e \leq e_{max} \\ 0 & e_{max} < e < 1 \end{cases} \quad (1)$$

A χ^2 minimization yields the best model parameters $e_{crit} = 0.25$ and $e_{max} = 0.92$. The χ^2 minimization applied to the more recent epoch eccentricity distribution (bottom panel of Figure 1), yields $e_{crit} = 0.0$ and $e_{max} = 0.91$. The relative increase in the number of low eccentricity planets discovered in the last year results in best parameters that are effectively a single-piece model.

Juric & Tremaine (2007) and Zhou et al. (2007) predict that the eccentricity distribution of dynamically active planetary systems approaches a Rayleigh-distribution due to planet-planet scattering, and they

show the Rayleigh-distribution is similar to the observed planet eccentricity distribution. The dotted curve in Figure 1 shows the Rayleigh-distribution with $\sigma_e = 0.3$ that best describes the outcome of the planet-planet scattering calculations from Juric & Tremaine (2007). The Rayleigh-distribution under represents the low eccentricity systems in the most recent eccentricity data. Juric & Tremaine (2007) based their study on the sample of planets known at the time (April 2006). Subsequently, relatively more planets with low eccentricities have been announced. In addition, Juric & Tremaine (2007) included systems with $P > 20$ day whereas this sample has $P > 10$ day. The dotted histogram in the lower panel of Figure 1 shows the eccentricity distribution at the most recent epoch (September 2007), but with systems with $P < 20$ day removed; apparently the difference is slight and will hereafter be ignored. Although this study concentrates on the two-piece model to describe the eccentricity distribution, results are also given for the Rayleigh-distribution with $\sigma_e = 0.3$. To provide results with the Rayleigh-distribution, the distribution is set to zero for $e > 0.95$.

3. TRANSIT PROBABILITY

Barnes (2007) derives the impact of orbital eccentricity on the probability for a planet to transit its stellar host (see also Seagroves et al. 2003). The probability to transit depends on the planet-star separation during transit. For an eccentric orbit, a transit occurring during pericenter enhances the transit probability and a transit occurring during apocenter decreases the transit probability. When averaged over observing angles, the net result is an enhancement of the probability to transit over the circular orbit case,

$$\text{Prob}_{Te} = \frac{\text{Prob}_{To}}{(1 - e^2)}, \quad (2)$$

where Prob_{To} is the transit probability of the circular orbit case (Barnes 2007). A planet with $e=0.6$ is ~ 1.5 times more likely to transit than a planet on a circular orbit.

With the observed eccentricity distribution from § 2, it is possible to calculate the average enhancement in the transit probability over the circular orbit case,

$$\langle \text{Prob}_{Te} \rangle = \int_0^1 \text{Prob}_{Te} P(e) de. \quad (3)$$

The resulting integral using Equation 1 for the eccentricity distribution is,

$$\begin{aligned} \langle \text{Prob}_{Te} \rangle = & \frac{\text{Prob}_{To}}{(e_{\max}^2 - e_{\text{crit}}^2)} [2(e_{\max} - e_{\text{crit}}) \text{arctanh}(e_{\text{crit}}) \\ & + \ln \left(\frac{(1 - e_{\max}^2)}{(1 - e_{\text{crit}}^2)} \right) + e_{\max} \ln \left(\frac{(1 - e_{\text{crit}})(1 + e_{\max})}{(1 + e_{\text{crit}})(1 - e_{\max})} \right)]. \end{aligned} \quad (4)$$

Using the numerical values for e_{crit} and e_{\max} from § 2, $\langle \text{Prob}_{Te} \rangle = 1.26$ and 1.23 for the earlier and current epochs of observed eccentricities, respectively. The Rayleigh distribution results in $\langle \text{Prob}_{Te} \rangle = 1.31$. Figure 2 illustrates $\langle \text{Prob}_{Te} \rangle$ for other choices of the eccentricity distribution model parameters. Figure 2 is a function of e_{\max} and the curves are for selected values of e_{crit} as labeled. Thus, it is expected that the yield from a transit survey that is sensitive to $P > 10$ day planets will be $\sim 25\%$

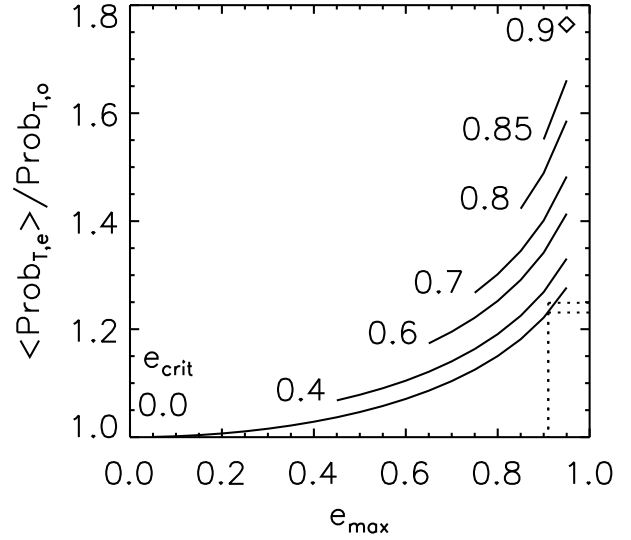


FIG. 2.— Average transit probability as a function of the observed eccentricity distribution model parameters. The transit probability is scaled to the equivalent transit probability for a circular orbit. The abscissa indicates e_{\max} , and the curves are for selected values of e_{crit} as labeled. For the model parameters shown in Figure 1, $\langle \text{Prob}_{Te} \rangle \sim 25\%$ higher than assuming all planets have circular orbits (dotted lines).

larger than expectations that assume circular orbits for all planets. This section discusses only the probability to transit, and it does not address whether the planet has a transit signal that is detectable. Thus, the results from this section assumes the enhanced probability for the planet to transit does not affect its detectability, which is the topic of the next section.

4. TRANSIT DURATION

4.1. Edge-on Transit

In addition to enhancing the probability for a transit to occur, orbital eccentricity results in the transit duration varying according to the planet's longitude of pericenter during transit. The transit duration is shortest (longest) if the transit occurs when the planet is at pericenter (apocenter) when transiting its stellar host. A short transit duration may reduce the detectability of the transit event. Assuming constant velocity during transit, the transit duration scaled to the edge-on ($i = 90^\circ$) circular orbit case has extrema of

$$\tau_{\pm}^e = \frac{t_{\pm}}{t_o} = \sqrt{\frac{(1 \mp e)}{(1 \pm e)}} \sim 1 \mp e + e^2/2, \quad (5)$$

where the sign on top and bottom corresponds to the pericenter and apocenter transit durations, respectively (Barnes 2007). When $e=0.6$, the transit duration at apocenter is twice the circular orbit case. Given the range of eccentricities observed for extrasolar planets with $P > 10$ day, we expect significant variations in the transit duration compared to that of a circular orbit.

Tingley & Sackett (2005) (their Equation 7) provides a simplified form of the transit duration, including longitude of pericenter, ϖ , and orbital inclination, i . In deriving the transit duration, (Tingley & Sackett 2005) assume constant orbital velocity and planet-star separation during transit and the planet crosses the stellar disk

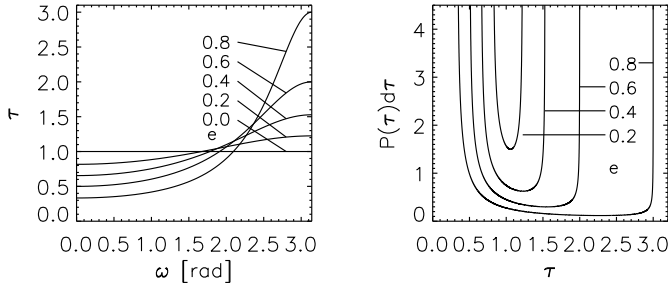


FIG. 3.— *Left:* Edge-on transit duration, τ , scaled to the edge-on circular orbit case as a function of the longitude of pericenter, ϖ , for several eccentricities as labeled. *Right:* For a uniform distribution of ϖ , solid curves show the distribution for transit duration scaled to the edge-on circular orbit case assuming all orbits are edge-on (i.e. $i = 90^\circ$).

along a straight path ($a \gg R_*$). An exact calculation (of a numerical nature given the need to solve Kepler's Equation) of the transit duration finds Equation 7 of Tingley & Sackett (2005) is accurate to better than 5% for $e=0.9$ and orbital separation $a \geq 0.1$ AU ($P \sim 10$ day). The equation is accurate to better than 1% for $e=0.9$ and $a \geq 1.0$ AU.

After scaling to the transit duration of the edge-on ($i = 90^\circ$), circular orbit with the same period and separation, Equation 7 of Tingley & Sackett (2005) becomes,

$$\tau = \frac{\sqrt{(1-e^2)}}{(1+e\cos(\varpi))} \sqrt{1 - \rho^2 \left[\frac{(1-e^2)}{(1+e\cos(\varpi))} \right]^2 \cos(i)^2}, \quad (6)$$

where $\rho = a/(R_* + R_p)$, R_* is the radius of the star and R_p is the radius of the planet. The definition for ϖ is with respect to the line of sight. Thus, $\varpi = 0$ means the pericenter is aligned with the observers line of sight, and $\varpi = 180^\circ$ means the apocenter is aligned with the observers line of sight. This varies from the definition of the argument of pericenter, ω , which is defined with respect to the line of nodes on the plane of the sky ($\varpi = \omega - 90^\circ$).

The $i = 90^\circ$ case illustrates the first order impact of orbital eccentricity on transit duration. In this case, Equation 6 simplifies to

$$\tau_{90^\circ} = \frac{\sqrt{(1-e^2)}}{(1+e\cos(\varpi))}. \quad (7)$$

The left panel of Figure 3 shows the transit duration with respect to the edge-on circular orbit case for a variety of orbital eccentricities as a function of ϖ . For a uniform distribution in ϖ , the shallow slope in transit duration at pericenter and apocenter results in a distribution of transit durations peaked at these extrema (given by Equation 5) with low probability for a transit duration in between these extrema.

Assuming a uniform distribution of ϖ , $p(\varpi)d\varpi = d\varpi/\pi$, the transformation law of probabilities (Equation 7.2.4 in Press et al. 1992) yields the distribution of transit durations,

$$p(\tau)d\tau = \left| \frac{\partial \varpi}{\partial \tau} \right| p(\varpi)d\varpi, \quad (8)$$

resulting in

$$p(\tau)d\tau = \frac{\sqrt{1-e^2}d\tau}{\pi\tau\sqrt{(e\tau)^2 - (\sqrt{1-e^2} - \tau)^2}}. \quad (9)$$

The right panel of Figure 3 shows the probability density for transit duration with $i = 90^\circ$ for various orbital eccentricities. As expected the probability density is heavily weighted toward the extrema. The singularities in the probability density at the extrema are integrable, making the probability density normalizable.

4.2. Affect of Varying Inclination Angle

The previous section shows the expected transit duration for fixed orbital eccentricity when the inclination angle, $i = 90^\circ$. Varying the inclination impacts the transit duration in two important ways. First, as the inclination decreases, the path of the planet across the stellar disc shortens, resulting in a reduction of the transit duration. Second, for an eccentric orbit, the planet is closer to the star at pericenter and farther away at apocenter. The smaller separation at pericenter increases the range of inclination angles that result in a transit, and conversely, a planet at apocenter will have a reduction in the range of inclination angles for a transit to occur. Thus, long transit duration events when the planet is at apocenter become increasingly rare as the eccentricity increases. This section quantifies these effects on the transit duration distribution.

Beginning with a simple joint distribution that is uniform in $\cos(i)$ and uniform in ϖ enables the more complicated distribution for transit duration to be derived. For this section, e remains fixed. The beginning joint distribution is,

$$P(\varpi, 0 \leq \cos(i) \leq \cos(i_{min})|e)d(\cos(i))d\varpi = Ad(\cos(i))d\varpi, \quad (10)$$

where $\cos(i_{min})$ is cosine of the minimum inclination angle necessary for a transit to occur, and A is the normalization constant. Setting $\tau = 0$ in Equation 6 and solving for $\cos(i)$ yields $\cos(i_{min}) = (1+e\cos(\varpi))/\rho(1-e^2)$. Integrating Equation 10 over the range of variables yields the normalization constant, $A = \rho(1-e^2)/\pi$.

The transformation law of probabilities for multiple dimensions (Equation 7.2.4 in Press et al. 1992) provides the joint probability density in terms of new variables τ and ϖ when starting with the probability density for $\cos(i)$ and ϖ .

$$P(\tau, \varpi|e)d\tau d\varpi = \left\| \frac{\partial \cos(i)}{\partial \tau} \frac{\partial \cos(i)}{\partial \varpi} \right\| P(\cos(i), \varpi)d\tau d\varpi, \quad (11)$$

In Equation 11, $\partial \varpi / \partial \tau = 0$ and $\partial \varpi / \partial \varpi = 1$. Thus, only $\partial \cos(i) / \partial \tau$ remains, and Equation 11 simplifies to

$$P(\tau, \varpi|e)d\tau d\varpi = \left| \frac{\partial \cos(i)}{\partial \tau} \right| \rho(1-e^2)/\pi d\tau d\varpi. \quad (12)$$

The requisite derivative needed in Equation 12 is obtained by solving Equation 6 for $\cos(i)$ yielding

$$\cos(i) = \frac{(1+e\cos(\varpi))}{\rho(1-e^2)^{3/2}} \sqrt{(1-e^2) - \tau^2(1+e\cos(\varpi))^2}, \quad (13)$$

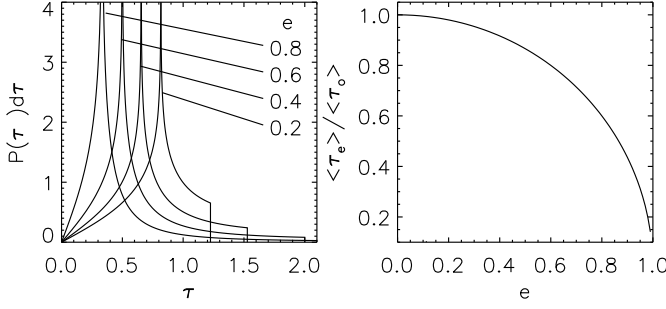


FIG. 4.— *Left*: Transit duration distribution scaled to the edge-on circular orbit case for a uniform distribution of $\cos(i)$ and fixed eccentricity. The cases $e=0.2, 0.4, 0.6$, and 0.8 are shown. *Right*: Average transit duration scaled to the average transit duration of a circular orbit as a function of orbital eccentricity (solid line).

$$P(0 \leq \tau \leq \tau_a, \varpi_{\min} \leq \varpi \leq \pi|e) d\tau d\varpi = \frac{\tau(1 + e \cos(\varpi))^3}{\pi \sqrt{1 - e^2} \sqrt{(1 - e^2) - \tau^2(1 + e \cos(\varpi))^2}} d\tau d\varpi, \quad (14)$$

where the lower limit to ϖ is necessary to avoid an imaginary result and is given by

$$\varpi_{\min} = \cos^{-1} \left[\text{MIN} \left(1.0, \frac{\sqrt{1 - e^2} - \tau}{\tau e} \right) \right]. \quad (15)$$

For $\tau \leq \tau_{\text{peri}}$, $\varpi_{\min} = 0$, but as $\tau > \tau_{\text{peri}}$, $\varpi_{\min} > 0$ since only transits occurring closer to apocenter result in a transit duration long enough.

Finally, the conditional probability density for transit duration alone is obtained by integrating over ϖ ,

$$P(\tau|e) d\tau = \int_{\varpi_{\min}}^{\pi} P(\tau, \varpi|e) d\tau d\varpi. \quad (16)$$

A solution to the above integral is possible in terms of a summation of the incomplete elliptic integrals of the first, second, and third kind (Byrd & Friedman 1954). In practice, I choose to solve the integral numerically, which is readily solved using the Romberg open ended algorithm which takes into account the singularity at the lower limit of integration at $\varpi = \varpi_{\min}$ (Press et al. 1992). Tests of convergence show Equation 16 has a singularity at $\tau = \tau_{\text{peri}}$, but it is integrable elsewhere over the range $0 \leq \tau \leq \tau_a$.

The left panel in Figure 4 shows the probability density for transit duration scaled to the edge-on circular orbit case at several values of eccentricity. By comparison to Figure 3, the main impact of orbital inclination is to strongly enhance the probability of observing a short duration event at pericenter relative to a long duration event at apocenter. The probability density also allows arbitrarily short events due to the potential for grazing events.

The probability density for transit duration can be summarized by finding the average transit duration at fixed eccentricity,

$$\langle \tau_e \rangle = \int_0^{\tau_a} \tau P(\tau|e) d\tau. \quad (17)$$

The right panel in Figure 4 shows $\langle \tau_e \rangle$ scaled to the average transit duration of the circular orbit case, $\langle \tau_0 \rangle = \pi/4$,

as the solid line. The function,

$$\langle \tau_e \rangle = \frac{\pi}{4} \sqrt{1 - e^2}, \quad (18)$$

fits the relation to better than 10^{-6} (similar to the numerical integration precision), which very strongly suggests this is the analytical solution to the integral in Equation 17. Tingley & Sackett (2005) find the same result in terms of the average value for their η parameter at fixed eccentricity (see their Equation 18).

4.3. Transit Duration Distribution For Observed Eccentricity Distribution

The previous section derives the transit duration distribution at fixed eccentricity. This section derives the transit duration distribution assuming planets follow the observed eccentricity distribution. As in the previous section, deriving the transit duration distribution begins with the simple distribution that is uniform in $\cos(i)$, uniform in ϖ , and the distribution of e follows the observed distribution as given in §2. The transformation law of probabilities enables transforming the simple distribution in $\cos(i)$, ϖ , and e into the distribution expressed in τ , ϖ , and e .

The initial distribution is given by,

$$P(0 \leq \cos(i) \leq \cos(i_{\min}), 0 \leq \varpi \leq \pi, 0 \leq e \leq e_{\max}) d\cos(i) d\varpi de = AP(e) d\cos(i) d\varpi de, \quad (19)$$

where the normalization constant $A = \rho\gamma/\pi$, where

$$\gamma = (e_{\max}^2 - e_{\text{crit}}^2) [2(e_{\max} - e_{\text{crit}}) \text{arctanh}(e_{\text{crit}}) + \ln \left(\frac{(1 - e_{\max}^2)}{(1 - e_{\text{crit}}^2)} \right) + e_{\max} \ln \left(\frac{(1 - e_{\text{crit}})(1 + e_{\max})}{(1 + e_{\text{crit}})(1 - e_{\max})} \right)]^{-1}. \quad (20)$$

The Jacobian transformation matrix simplifies as before, such that the transit duration distribution scaled to the edge-on, circular orbit transit duration is given by,

$$P(0 \leq \tau \leq \tau_a, \varpi_{\min} \leq \varpi \leq \pi, e_{\min} \leq e \leq e_{\max}) d\tau d\varpi de = \left| \frac{\partial \cos(i)}{\partial \tau} \right| P(\cos(i), \varpi, e) d\tau d\varpi de, \quad (21)$$

where the lower limit to the eccentricity, e_{\min} , becomes necessary for $\tau > 1$, when too small of an eccentricity cannot produce a transit duration as long as τ . Solving τ_a for e yields $e_{\min} = \text{MAX}[0.0, (\tau^2 - 1)/(\tau^2 + 1)]$. Overall, the joint distribution is given by

$$P(\tau, \varpi, e) d\tau d\varpi de = \frac{\gamma P(e)}{\pi} \frac{\tau(1 + e \cos(\varpi))^3}{(1 - e^2)^{3/2} \sqrt{1 - e^2 - \tau^2(1 + e \cos(\varpi))^2}} d\tau d\varpi de. \quad (22)$$

Integrating over ϖ and e provides the final probability density for τ for the assumed distribution of orbital eccentricities. Given the additional complication of integration over two variables, an analytical solution was not forthcoming. As in § 4.2, the singularities in the integrand are integrable, and the Romberg open ended algorithm which takes into account the singularity at the

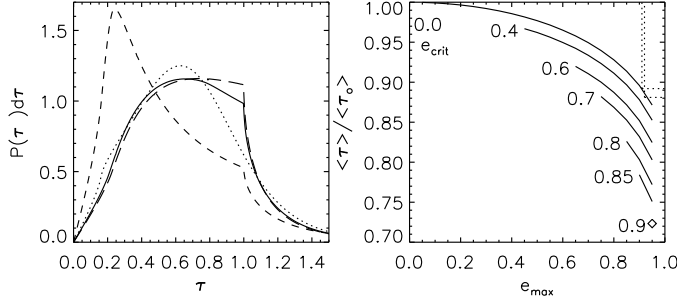


FIG. 5.— *Left:* Transit duration distribution scaled to the edge-on circular orbit case for a uniform distribution of $\cos(i)$ and the observed distribution of e as shown in the top panel (*solid line*) and bottom panel (*long dashed line*) of Figure 1. Given the bias against detecting high eccentricity planets in radial velocity surveys, a uniform distribution of orbital eccentricities up to high eccentricity ($e_{\text{crit}} = 0.9$ and $e_{\text{max}} = 0.95$) will be highly skewed towards $\tau \sim 0.3$ (*short dashed line*). A Rayleigh distribution of orbital eccentricities results in relatively fewer transit durations $\tau \sim 1$ due to the relatively fewer objects on circular orbits (*dotted line*). *Right:* Average transit duration scaled to the average transit duration of a circular orbit as a function of the observed eccentricity distribution model parameters. The abscissa indicates e_{max} , and the curves are for selected values of e_{crit} as labeled. For the model parameters shown in Figure 1, $\langle \tau \rangle \sim 0.88$ times shorter than assuming all planets have circular orbits (*dotted line*).

lower limits of integration (Press et al. 1992) provides the solution.

The solid and long-dashed lines in Figure 5 shows the distribution of transit duration scaled to the edge-on circular orbit case for a population of extrasolar planets that follows the observed orbital eccentricity distributions shown in top and bottom panels of Figure 1, respectively. The probability density has a broad flat top with $\tau = 0.4$ just as likely to occur as $\tau = 1.0$. For comparison, the transit duration distribution that would result from a nearly uniform distribution of orbital eccentricity up to high eccentricities ($e_{\text{crit}} = 0.9$ and $e_{\text{max}} = 0.95$) is shown as the short-dashed line in Figure 5. Given the bias against detecting $e > 0.6$ extrasolar planets in radial velocity studies (Cumming 2004), a large population of $e \sim 0.9$ planets cannot be ruled out. The transit duration distribution resulting from the Rayleigh distribution of orbital eccentricity (dotted line in Figure 5) has relatively fewer planets with $\tau \sim 1$ due to its relatively fewer circular orbits.

In the future, if a statistically large sample of transiting planets with orbital $P > 10$ days is available with accurate stellar parameters, histograms of observed transit duration scaled to the edge-on circular orbit case may help characterize the underlying eccentricity distribution. After accounting for the selection effects, a large number of $\tau \sim 0.3$ detections relative to $\tau \sim 0.8$, as illustrated in the right panel of Figure 5, would indicate $e = 0.9$ planets are as common as circular orbits. Work toward understanding the sensitivity of Kepler for constraining the underlying eccentricity distribution is underway (E. Ford, private communication).

The right panel of Figure 5 summarizes the transit duration distribution by showing $\langle \tau_e \rangle$ in terms of the parameters characterizing the eccentricity distribution, e_{crit} and e_{max} . Each line corresponds to a fixed value of e_{crit} as labeled, and the abscissa indicates e_{max} of the eccentricity distribution. For the eccentricity distribution in

the top panel of Figure 1 $\langle \tau_e \rangle / \langle \tau_o \rangle = 0.88$ and the bottom panel $\langle \tau_e \rangle / \langle \tau_o \rangle = 0.89$. The Rayleigh distribution results in $\langle \tau_e \rangle / \langle \tau_o \rangle = 0.86$

5. DISCUSSION: APPLICATION TO TRANSIT SURVEYS

The results from § 4 quantify the impact orbital eccentricity has on the transit duration. Overall, orbital eccentricity results in shorter transit durations than the circular orbit case, and the short transit duration reduces the transit detectability. This section quantifies the reduction in transit detectability for various noise models of transit surveys.

In a transit survey with independent photometric measurements, the transit signal to noise ratio is,

$$\text{SNR} = \frac{\Delta F}{\sigma} \sqrt{N_{\text{obs}}}, \quad (23)$$

where ΔF is the transit depth (the transit is modeled as a box-car shape), σ is the error on a photometric measurement, and N_{obs} is the number of measurements during one or more transit(s). A shorter transit duration reduces $N_{\text{obs}} \propto \tau$, thus, $\text{SNR} \propto \sqrt{\tau}$. The observed eccentricity distribution (Figure 1) results in $\bar{\tau} = \langle \tau_e \rangle / \langle \tau_o \rangle = 0.88$, and on average the reduced transit duration results in an effectively smaller $\text{SNR}_{\text{eff}} = \sqrt{\bar{\tau}} = 0.94$ per transit than assuming all planets are on circular orbits.

The above impact on the transit signal SNR due to a shorter transit duration is for an individual star in a survey. However, the reduced SNR will have a larger impact on the overall transit detectability in an ideal field transit survey. As described in Gaudi et al. (2005) and Gaudi (2007), a specified SNR criteria for transit detection, SNR_{min} , in a field transit survey corresponds to a maximum distance, $\ell_{\text{max}} \propto \text{SNR}_{\text{min}}^{-1}$, out to which a planet is detectable. This proportionality assumes white noise and the dominant source of photometric error is Poisson noise. In the studies of Gaudi et al. (2005) and Gaudi (2007), ℓ_{max} is a function of the planet radius and stellar host spectral type (i.e. ℓ_{max} is a smaller distance for a smaller radius planet or larger radius star). For this study only the dependence of ℓ_{max} on transit duration is of interest.

Overall, the yield from a transit survey is proportional to the number of objects in the survey that meets SNR_{min} , which is $N_{\text{obj}} \propto \ell_{\text{max}}^3$ for stars distributed uniformly in the survey volume as appropriate for nearby stars. The effective $\text{SNR}_{\text{min,eff}} = \text{SNR}_{\text{min}} \sqrt{\bar{\tau}}$ larger than assuming all planets are on circular orbits. Thus, the number of objects in an idealized transit survey where a transit is detectable is $N_{\text{obj,e}} = \bar{\tau}^{3/2} N_{\text{obj,o}} = 0.82 N_{\text{obj,o}}$ times smaller than the case where the detectability of a transit is based on assuming all planets have circular orbits, $N_{\text{obj,o}}$. Despite the reduced detectability of transits, this is offset by the higher probability for the planet to transit in the case of significant eccentricity § 3. The overall yield of the idealized transit survey is discussed in § 6 taking both the reduced detectability and enhanced probability to transit into account.

In practice, transit surveys typically are affected by correlated measurements (Pont et al. 2006). In this regime, the correlation time scale is similar to the transit duration and repeated measurements do not add independent information. When correlated measurements dominate the photometric error, the $\text{SNR} =$

$(\Delta F/\sigma_{\text{cor}})\sqrt{N_{\text{tr}}}$, where N_{tr} is the number of transits detected, and the correlated measurement error, σ_{cor} , no longer depends on the stellar luminosity, but is constant (Gaudi 2007). When dominated by correlated measurements, the SNR is independent of τ and the only requirement is to have a short enough sampling cadence to detect the shortest transit duration expected. Thus, a shorter τ due to orbital eccentricity has no impact on the transit detectability in a survey which is dominated by correlated measurements (i.e. $N_{\text{obj,e}} = N_{\text{obj,o}}$). However, the Poisson limited, white noise transit survey will have a higher planet yield than a survey dominated by correlated measurements (Pont et al. 2006), but in the latter case, orbital eccentricity does not impose any additional reduction in the transit detectability.

The Kepler space-based transit survey whose goal is to detect several Earth-sized planets (Borucki et al. 2004) contends with stellar intrinsic variability as the dominant source of noise (Jenkins 2002). Using integrated flux measurements of the Sun to model intrinsic variability of stars, Jenkins (2002) characterizes the detectability of Earth-sized transiting planets with Kepler. The Sun has low noise on 7 hr time scales typical of transiting Earth-sized planets in 1 yr orbital periods. However, the solar noise increases by ~ 4 orders of magnitude by 10 day time scales (see Figure 2 of Jenkins 2002). The rapidly increasing intrinsic noise toward longer time scales cancels any benefit of increased transit signal SNR for transit durations >4 hr for the Kepler mission (see Figure 9 of Jenkins 2002). Thus, as long as the transit duration remains above 4 hr, orbital eccentricity will not reduce the detectability of Earth-sized planets with Kepler.

6. CONCLUSION

Orbital eccentricity results in an enhanced probability for a planet to transit and potentially a reduction in the transit detectability. The overall yield from a transit survey is given by $N_{\text{det}} \propto \text{Prob}_T \times N_{\text{obj}}$. The results from this study can be used to scale the overall yield from a transit survey based on assuming all planets are on circular orbits for an assumed distribution of orbital eccentricity. The enhanced probability for a planet to transit, Prob_T with a distribution of orbital eccentricity scaled to the circular orbit case is given by Equation 4. The reduced number of transiting planets detectable N_{obj} scaled to the circular orbit case for an ideal transit survey where the photometric noise is white and dominated by Poisson error is given in § 5. Multiplying these two factors provides the overall yield of an ideal transit survey scaled to assuming all planets are on circular orbits. Figure 6 show that these two opposing effects nearly cancel over the parameters that characterize the eccentricity distribution. Thus, for an idealized transit survey with the currently observed orbital eccentricity distribution, the overall yield will be 4% greater than assuming all planets are on circular orbits. The result for an idealized transit survey with a Rayleigh distribution of orbital eccentricities gives a similar enhancement (4%).

In ground-based transit surveys, correlated measurements limit transit detectability (Pont et al. 2006) and intrinsic variability of the star will limit the detectability for Earth-sized planets for the Kepler mission (Jenkins 2002). In both cases the transit detectability is inde-

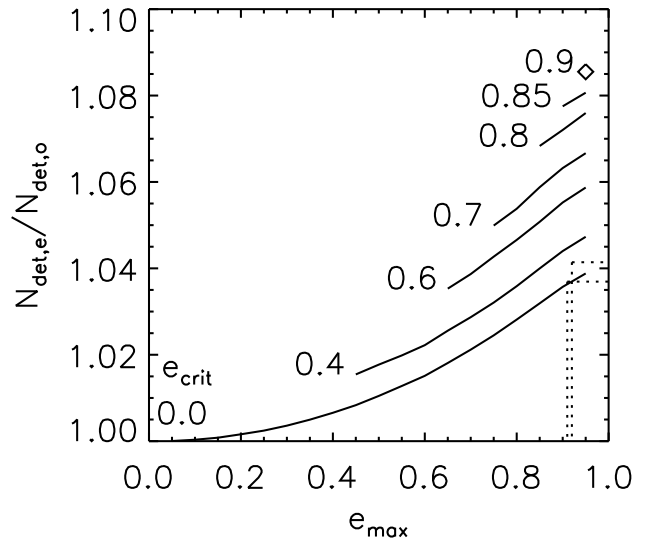


FIG. 6.— The overall yield from an idealized transit survey as function of the observe eccentricity distribution model parameters scaled to the assumption that all planets have circular orbits. The transit survey is assumed to have independent photometric measurements that are dominated by Poisson noise. The abscissa indicates e_{max} , and the curves are for selected values of e_{crit} as labeled. For the model parameters shown in Figure 1, $N_{\text{det}} \sim 4\%$ higher than assuming all planets have circular orbits (dotted line).

pendent of the transit duration, in which case N_{obj} is independent of the orbital eccentricity. For these cases, the transit survey will have higher returns by a factor of $\langle \text{Prob}_T \rangle$ (Equation 4) than estimated by assuming all planets are on circular orbits. However, the reduced planet yield in a transit survey due to intrinsic stellar variability or correlated measurements must be properly accounted for. If every dwarf star has an Earth-sized planet orbiting in the habitable zone, then assuming circular orbits, the Kepler mission expects to detect 100 Earth-sized planets in the habitable zone (Borucki et al. 2004). The work presented here indicates Kepler will have $\langle \text{Prob}_T \rangle \sim 25\%$ higher yield if Earth-sized planets in the habitable zone have a planet eccentricity distribution similar to the currently known sample of giant planets from radial velocity surveys. However, if Earth-sized planets with $e \sim 0.9$ are as common as $e \sim 0$ then, the yield of Earth-sized planets could be 80% higher from the Kepler mission assuming the high- e , short transit duration planets are still detectable.

The dependence of the transit survey yield on the uncertain underlying orbital eccentricity distribution implies an uncertainty in measuring the frequency of terrestrial planets in the habitable zone (a major goal of the Kepler mission Borucki et al. 2004). An analysis of the transit yield from a transit survey that assumes all planets are on circular orbits will overestimate the frequency of habitable planets if high eccentricities are common and not taken into account. In practice a variety of noise regimes affect a transit survey and accurate yields necessitate an accurate understanding of the photometric noise, stellar sample, and underlying eccentricity distribution (Burke et al. 2006; Gould et al. 2006; Fressin et al. 2007).

This paper benefited from discussions with Scott Gaudi, Will Clarkson, Peter McCullough, and Eric

Ford. This work is funded by NASA Origins grant NNG06GG92G.

REFERENCES

- Barbieri, M., et al. 2007, ArXiv e-prints, 710, arXiv:0710.0898
- Barnes, J. W. 2007, ArXiv e-prints, 708, arXiv:0708.0243
- Bordé, P., Rouan, D., & Léger, A. 2003, A&A, 405, 1137
- Borucki, W., et al. 2004, Second Eddington Workshop: Stellar Structure and Habitable Planet Finding, ESA SP-538, Noordwijk: ESA Publications Division, 177
- Burke, C. J., Gaudi, B. S., DePoy, D. L., & Pogge, R. W. 2006, AJ, 132, 210
- Butler, R. P., et al. 2006, ApJ, 646, 505
- Byrd, P. F., & Friedman, M. 1954, Mitteilungen der Astronomischen Gesellschaft Hamburg, 5, 99
- Cresswell, P., Dirksen, G., Kley, W., & Nelson, R. P. 2007, ArXiv e-prints, 707, arXiv:0707.2225
- Cumming, A. 2004, MNRAS, 354, 1165
- Fischer, D. A., et al. 2007, ApJ, 669, 1336
- Ford, E. B., & Rasio, F. A. 2007, ArXiv Astrophysics e-prints, arXiv:astro-ph/0703163
- Fressin, F., Guillot, T., Morello, V., & Pont, F. 2007, ArXiv e-prints, 704, arXiv:0704.1919
- Gaudi, B. S. 2007, in Michelson Summer Workshop 2007, (Moffett Field, CA: NASA Ames Conf. Center) http://msc.caltech.edu/workshop/2007/Gaudi_stat.pdf
- Gaudi, B. S., Seager, S., & Mallen-Ornelas, G. 2005, ApJ, 623, 472
- Goldreich, P., & Tremaine, S. 1980, ApJ, 241, 425
- Gould, A., Dorsher, S., Gaudi, B. S., & Udalski, A. 2006, Acta Astronomica, 56, 1
- Jenkins, J. M. 2002, ApJ, 575, 493
- Jones, H. R. A., Butler, R. P., Tinney, C. G., Marcy, G. W., Carter, B. D., Penny, A. J., McCarthy, C., & Bailey, J. 2006, MNRAS, 369, 249
- Juric, M., & Tremaine, S. 2007, ArXiv Astrophysics e-prints, arXiv:astro-ph/0703160
- Moutou, C., Pont, F., & Halbwachs, J.-L. 2006, Formation planétaire et exoplanètes, Ecole thématique du CNRS, Goutelas (Loire), 23 - 27 mai 2005 Edited by J.-L. Halbwachs, D. Egret, and J.-M. Hameury. Strasbourg: Observatoire astronomique de Strasbourg et Société Française d'Astronomie et d'Astrophysique (SF2A), 2006, p. 55-79 <http://astro.u-strasbg.fr/goutelas/g2005/>, 28, 55
- Naef, D., et al. 2001, A&A, 375, L27
- Pont, F., Zucker, S., & Queloz, D. 2006, MNRAS, 373, 231
- Press, W. H., Teukolsky, S. A., Vetterling, W. T., & Flannery, B. P. 1992, Cambridge: University Press, —c1992, 2nd ed.
- Raymond, S. N., Quinn, T., & Lunine, J. I. 2006, Icarus, 183, 265
- Ribas, I., & Miralda-Escudé, J. 2007, A&A, 464, 779
- Seagroves, S., Harker, J., Laughlin, G., Lacy, J., & Castellano, T. 2003, PASP, 115, 1355
- Tamuz, O., et al. 2007, A&AL, in press (astro-ph/0710.5028)
- Tingley, B., & Sackett, P. D. 2005, ApJ, 627, 1011
- Zhou, J.-L., Lin, D. N. C., & Sun, Y.-S. 2007, ApJ, 666, 423